Microscopic diffusion model applied to C60 fullerene fractals in carbon disulphide solution

Alok D. Bokare and Archita Patnaik

Citation: J. Chem. Phys. **119**, 4529 (2003); doi: 10.1063/1.1594177
View online: http://dx.doi.org/10.1063/1.1594177
View Table of Contents: http://jcp.aip.org/resource/1/JCPSA6/v119/i8
Published by the American Institute of Physics.

Microscopic diffusion model applied to C_{60} fullerene fractals in carbon disulphide solution

Alok D. Bokare and Archita Patnaik[a)]
Department of Chemistry, Indian Institute of Technology Madras, Chennai-600036 India

(Received 28 January 2003; accepted 2 June 2003)

Using Positronium (Ps) atom as a fundamental probe that maps changes in the local electron density of the microenvironment and high resolution transmission electron microscopy, C_{60} aggregation in neat CS_2 solvent is reported over a concentration range 0.02 to 2.16 g/dm^3. Spontaneous formation of stable spherical C_{60} aggregates in the colloidal range (~90–125 nm) was observed over a critical concentration range of 0.06–0.36 g/dm^3, beyond which the clusters broke. Specific interactions of the Ps atom with the surrounding revealed the onset concentration for stable aggregate formation in this solvent to be 0.06 g/dm^3. The solution phase C_{60} structure in the critical concentration range was analyzed to be a spherical fractal aggregate with a fractal dimension of 1.9 and the growth mode followed a diffusion limited cluster aggregation mechanism. At concentrations beyond 0.36 g/dm^3, an entropy driven phase change was noticed leading to the formation of irregular, but oriented crystalline components. A microscopic diffusion model was applied to calculate the o-Ps lifetime density function and diffusion coefficients of o-Ps and the C_{60} aggregates in the solution. With randomly distributed C_{60} fractal clusters, the o-Ps density function resulted in a good agreement between the calculated and the experimental o-Ps lifetimes, revealing the diffusion coefficients of C_{60} fractal cluster and the o-Ps to be 2.27×10^{-6} cm^2/s and 25.1×10^{-5} cm^2/s respectively.
 [DOI: 10.1063/1.1594177]

I. INTRODUCTION

With a similar magnitude of the specific surface energies of interaction amongst the C_{60} and the solvent molecules, the fullerene molecules in solution display a trend towards aggregate/cluster formation.[1–8] The nonmonotone temperature dependence of solubility[9] and the solvatochromic effect[10,11] are to name a few. A thermodynamic approach to the description of cluster formation in C_{60} solutions was put forward based on the droplet model of a cluster.[12] Based on modern approaches to the description of mechanism of fractal cluster growth, Ying *et al.*[3] showed a slow aggregation of C_{60} in neat dilute benzene in a concentration range 0.78–1.39 mg/ml at room temperature to be reversible. The DLS intensity indicated the aggregates to be fractals of dimension 2.10, with the aggregation kinetics exhibiting an essentially exponential behavior. The fractal growth of C_{60} aggregates followed a reaction limited cluster aggregation (RLCA) mechanism emphasizing that the mass of aggregates grew with time. Slow C_{60} aggregation in neat toluene over a fairly dilute concentration range 0.18–0.78 g/l has also been studied both experimentally and theoretically[6] at room temperature. The aggregation kinetics described the clusters to be fractals with stable $(C_{60})_n$ clusters of sizes >1.2 nm and aggregation number $n \geqslant 3$. Extensive work on aggregation of C_{60}, C_{70}, and their mixture in a number of solvent mixtures has been reported.[11,13] Recently, Alargova *et al.*[4] confirmed stable and durable colloidal dispersions in these systems and established repulsive electrostatic interactions between the particles to be the origin of their stability. The most recent work of Yevlampieva *et al.*[8] reports C_{60} aggregation in neat N-methyl pyrrolidone using spectral and electro-optical methods. Our recent work[14] on C_{60} aggregation in neat CS_2 solvent determined the onset concentration for stable C_{60} aggregate formation to be 0.06 g/dm^3, beyond which the clusters broke down with further structural reorganization of the medium. While recalling this work, the present investigation focuses on application of a microscopic diffusion model to the stable aggregated C_{60} clusters, whereby the interaction process of o-Ps with the fullerene aggregates is revealed quantitatively.

II. EXPERIMENT

A. Materials

C_{60} of 99.5+% purity was purchased from MER Corporation, USA and the purity was confirmed through HPLC and Mass spectrometry. Carbon disulphide (Analytical Grade, SRL Chemicals, India) was freshly distilled and dried over molecular sieves prior to use. C_{60} solutions in the concentration range 0.02–2.16 g/dm^3 were prepared by ultrasonication and degassed to remove the dissolved oxygen. These concentrations were much below the saturation concentration/solubility limit[2] in CS_2 (7.92 g/dm^3 ≈ 7.9 mg/ml). During the acquisition of the spectra, no visible color change in the solutions was observed. Bezmel'nitsyn[2] reported that at concentrations three orders of magnitude less than the saturation limit (at ~0.007 g/dm^3), practically no clusters exist in the

[a)]Author to whom correspondence should be addressed. Present Address: JSPS Fellow, Department of Materials Technology, Chiba University, Chiba 263-8522 Japan. Fax: 043-290-3449; Electronic mail: archita59@yahoo.com

fullerene solution and contains only the isolated C_{60} molecules.

B. Positron annihilation spectroscopy

Positron lifetime spectra were recorded by a fast–fast timing coincidence system consisting of BaF_2 scintillation detectors with a timing resolution of 300 ps full width at half maximum (FWHM) for a Co-60 prompt. The positron source was ~15 μCi of ^{22}Na–acetate sandwiched and sealed in thin Al foils (2.5 μm thickness). All measurements were performed at room temperature (22 ± 1 °C). The lifetime spectra in our experiments was obtained as a combination of 3 exponentials as

$$y(t)=N_S\sum_{i=1}^{n}\alpha_i\lambda_i I(t)^*\exp(-\lambda_i t), \quad (1)$$

where α_i represents the probability of different annihilation channels and $I(t)$ represents the instrumental resolution function. The asterix (*) sign indicates a convolution of the 2 terms. The lifetime spectra were resolved into three exponentially decaying components by the PATFIT[15] program. The o-Ps lifetime and intensity are represented as τ_3 and I_3, respectively.

C. Transmission electron microscopy

HRTEM measurements and electron diffraction studies of the solutions were performed using a Philips STEM instrument (Model SM12) equipped with a field emission gun operated at 120 kV. Microfilms for TEM studies were prepared by placing a drop of the solution on a carbon coated copper grid and then drying of the solvents by evaporation at ambient temperature. Samples were then transferred to the microscope in a special vacuum transfer sample holder.

III. RESULTS AND DISCUSSION

A. TEM of C_{60} fullerene aggregates in the concentration range 0.06–0.36 g/dm^3

Figures 1(a) and 1(b) represent images at two different concentrations, 0.06 and 0.36 g/dm^3 of C_{60} aggregates. The pictures show spherical clusters whose average size was seen to decrease with concentration. At 0.06 g/dm^3 concentration, a cluster size of 125 nm is observed as opposed to a cluster size of 90 nm seen at 0.36 g/dm^3 concentration. The structure looks spherical with rodlike tails protruding outwards, making possible the attachment of one fullerene molecule with the other. A complete removal of C_{60} molecules from the solution to the aggregate form could not be achieved indicating an equilibrium between them as $mC_{60}\overset{K_m}{\leftrightarrow}(C_{60})_m$. Also, in the viewed grid region, the cluster size variation is more prominent for the latter, i.e., $(C_{60})_m$, in Fig. 1(b) as compared to that for the 0.06 g/dm^3 concentration [Fig. 1(a)], where a narrow distribution is observed. As a comparison, the TEM image of the 0.02 g/dm^3 solution (Fig. 2) shows a C_{60} monomeric species, whose presence is confirmed from the visible and well-arranged unidirectional crystal planes, indicating it to be an isolated single crystal. The size of the crystallite is 90 nm and the average center-to-center distance between the fullerene molecules is estimated to be about 0.7 nm. Electron diffraction of these clusters taken from the same area as the image showed a diffused pattern.[14] Presence of a diffused ring rather than discrete spots suggests that the microdomains within the cluster do not arrange themselves in a crystalline structure pattern and that the clusters are randomly oriented. Amorphous fractal aggregates have been observed previously in inorganic systems like fumed silica,[16] titania,[17] and aerosols.[18]

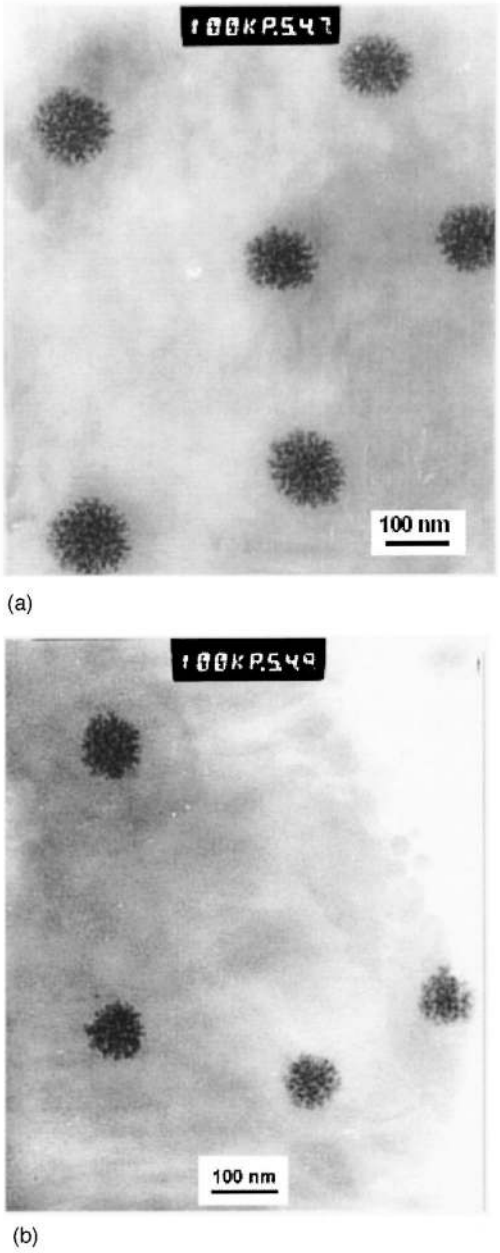

FIG. 1. (a) TEM image of the 0.06 g/dm^3 C_{60} solution microfilm at a higher magnification (100 K X) showing the microdomains within the spherical aggregate. (b) TEM micrograph of the 0.36 g/dm^3 C_{60} solution microfilm at 100 K X magnification.

B. Mechanism of C_{60} cluster growth

The TEM micrograph of the initial dilute 0.02 g/dm^3 C_{60} solution (Fig. 2) shows virtually no difference from that of

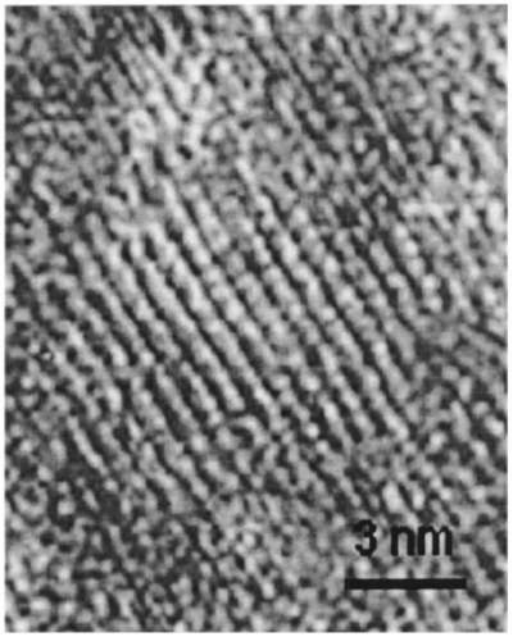

FIG. 2. HRTEM image of a fullerene monomer in the 0.02 g/dm^3 C_{60} solution microfilm.

the C_{60} molecular state. Changes appear with increasing concentration. The appearance of spherical clusters in the conc. range 0.06–0.36 g/dm^3 thus implies an associative mechanism to dominate at high C_{60} concentrations that governs the intermolecular interactions in these solutions. Association of C_{60} to form aggregates in CS_2 solution, its size, and the critical concentration of its formation can be explained in terms of a size-dependent free energy of aggregation; the latter is a cumulative of $C_{60}-C_{60}$ attractive (van der Waals forces) and repulsive electrostatic interactions; electrophoretic mobility measured and ξ-potential calculated for C_{60} colloidal dispersion in acetonitrile–toluene mixture have been reported[4] to be -3.30×10^{-4} cm^2/V s and -32.5 mV, respectively. The equilibria between the monomeric C_{60} and its aggregates of variable size $(C_{60})_m$ could be associated with a set of equilibrium constants, $K_m=[(C_{60})_m]/[C_{60}]^m$ and the free energy of aggregation is equivalent to the free energy of transfer, ΔG_m^0 of a simple C_{60} molecule from monomeric state to aggregate of size m. Thus, $-\mathrm{RT}\ln K_m = m\Delta G_m^0$ where ΔG_m^0 is a function of the environmental variables and the aggregate size. The dependence of the aggregate size on the total C_{60} concentration is closely linked to the size distribution function. Since the size varied in a narrow range (125–90 nm), the size distribution is not very prominent in our TEM images. Nevertheless, the effect of concentration on the size at the critical concentration of aggregation (0.06 g/dm^3) revealed a much steeper size distribution, observable in the TEM image as almost similar size aggregates. In micellar environments, at critical micellar concentration, a broader distribution was observed.[19]

C. Fractal nature of the C_{60} aggregate

Aggregation studies of colloids, e.g., colloidal polystyrene latex spheres,[20,21] colloidal silica,[22] etc. have served as model systems for describing the fractal nature of the aggregates present, where a correlation between the fractal mass and size could be attributed as $R=\alpha N^{1/d}$, where R was the cluster size, N, the number of primary particles in the aggregate, α, the lacunarity constant and d, the fractal dimension. The 2 limiting regions of irreversible colloids, namely, the reaction limited cluster aggregation (RLCA) and the diffusion limited cluster aggregation (DLCA) have been used to arrive at the structure and kinetics of these aggregates. The former is a slow aggregation process and is dependent on the time taken for particles to overcome a repulsive energy barrier by thermal activation. The fractal dimension in this case has been found to be 2.1 and the kinetics followed an exponential behavior. In the DLCA model, aggregation is a fast process between similar size particles and depends on the time taken for the particles to encounter each other by diffusion and the fractal dimension has been obtained as 1.8. The very first computer simulation for growth of aggregates through diffusion limited random walk of primary particles was put forward by Meakin[23] with a fractal dimension $d=2.5$. For the instantaneously formed mass-clusters at and beyond the $[C]_{\mathrm{critical}}$, we estimated the fractal dimension to be 1.9. Although the magnitude is higher than the general value of 1.8, owing to a similar size of the clusters as seen in Figs. 1(a) and 1(b) and the observed fast aggregation, we attribute the growth process to be governed by DLCA. Fractal dimensions for colloidal dispersions of fluorinated polymer particles, studied by small angle neutron scattering, have been found to be 1.9 in the framework of DLCA.[24] Mass fractal structures proposed for organic pigments studied by small angle x-ray scattering have been associated with $d=2.5$, discussed under RLCA.[17] Under the DLCA model, electrodeposited polypyrrole aggregates have been attributed with $d=2.5$. When variability of the diffusion coefficient with particle size and transport regime were considered in more complicated simulations, Mountain[25] found fractal dimensions of 1.89–2.07 for DLCA. Das *et al.*[26] reported $d=1.3$ for N^+ beam induced formation of graphitic clusters through DLCA in poly(*p*-phenylene oxide) matrix. Variation in the d value is thus visualized depending on the embedding dimension and the statistical nature of the structure of a cluster. The aggregation number (n) for the fractal clusters at different concentrations were calculated according to, $n=(R/r_0)^d$ and the values are listed in Table I.

TABLE I. Characteristics of C_{60} fractal cluster aggregates.

$[C_{60}]$ in CS_2 (g/dm^3)	C_{60} aggregate size (R_c) (nm)	Aggregation number (n)
0.06	125	3.2×10^4
0.14	110	2.5×10^4
0.36	90	1.7×10^4

D. C_{60} solution phase structure in the range (0.36<conc.≤2.16) g/dm^3

At concentrations >0.36 g/dm^3, [cf. Figs. 3(a) and 3(b)], the clusters further agglomerate to give looser flowerlike structures with an open hole in the center, upon further ad-

(a)

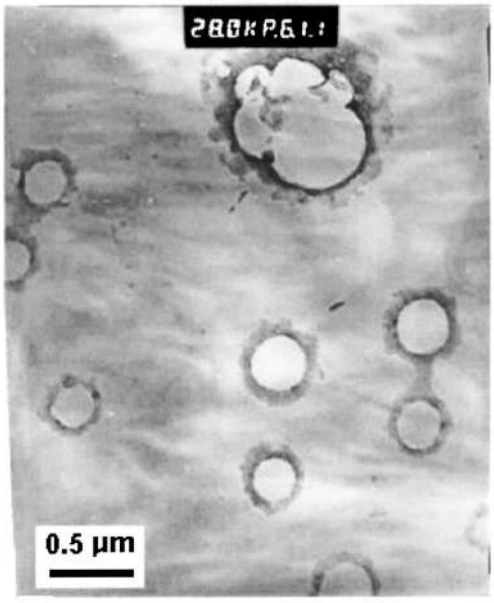

(b)

FIG. 3. (a) TEM micrograph of the 2.16 g/dm^3 C_{60} solution microfilm depicting the presence of agglomerated flowerlike structures with an open hole in the center. (b) TEM image of the 2.16 g/dm^3 C_{60} solution microfilm showing formation of fused open-clusters with hollow cores.

dition of single C_{60} molecules. Also observed are the fused open-clusters with hollow cores of size varying between 350 and 460 nm. Although inhomogeneously distributed, the molecular aggregates are held together via weak van der Waals forces when dispersed in the solution. This further complexity in the microphase/structure reorganization/phase separation is unanticipated and we attribute this to a phase transition of the system. These transitions have analogous counterparts in colloidal solutions where the most commonly observed phase transition is solidification with formation of a

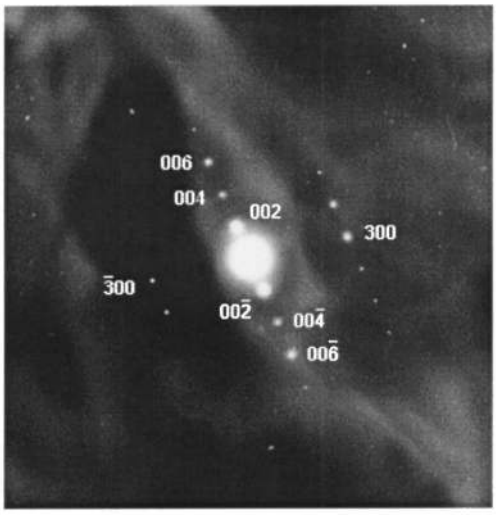

FIG. 4. Microdiffraction pattern of the agglomerated flowerlike cluster in the 2.16 g/dm^3 C_{60} solution microfilm.

condensed phase with regular crystal structure, formed upon a change in the external condition.[27] Figure 4 shows the electron diffraction pattern of one of the flowerlike structures to be highly oriented with discrete diffraction spots. The structural anisotropy may be accompanied by the long-range interactions playing a significant role. Structural analysis resembled the hexagonal close packing (hcp) lattice structure, analogous to that shown by C_{60} fullerites grown from a benzene solution.[28]

We explain this phase behavior at concentrations >0.36 g/dm^3 to be entropically driven by steric repulsion between the particles, complying with the fact that they are negatively charged.[4] Entropy maximization occurs by minimizing free energy $G=U-TS$ with U, the internal energy$=0$ for hard and impenetrable particles.[29] Entropically driven microphase transitions in mixtures of colloidal rods and spheres have been discussed where it is assumed that attractive interactions are necessary to generate phases with long range order.[30] The physical origin of the phase separation may be explained as: When the components phase-separate, the free volume of the suspension is maximized which precedes the raising of the translational entropy of the molecules at the expense of lowering the entropy of mixing. At low concentrations, entropy mixing dominates and the solution is miscible. But at high concentration, with gain in free volume, phase separation occurs with a repulsive interparticle potential.

E. Positron annihilation spectroscopy

This technique employs Positronium (Ps) atom, a bound state of free positron (e^+) and an electron (e^-), as a novel fundamental probe. Ps annihilates by emitting γ-quanta in 0.125 ns from the para-Ps (p-Ps) state and in 140 ns from the ortho-Ps (o-Ps) state. In the condensed phase, owing to the difference in the intrinsic lifetimes, the ortho-para conversion through electron exchange with the medium and spin conversion in the presence of internal or external magnetic field affects the o-Ps lifetime, reducing it to $\sim$1–10 ns in liquid

phase depending on the matrix structure and composition. The o-Ps mean lifetime (τ) is the inverse of the Ps annihilation rate (λ) and is given by the overlapping integral of the positron density and electron density (ρ_{el}) at the site of annihilation, as given below, where r_e is the classical electron radius, Ψ_{e^+} is the positron wave function and c is the velocity of light. Here R denotes the thickness of the electron layer, where annihilation takes place.

$$\frac{1}{\tau}=\lambda=\pi r_e^2 c\int_0^R |\psi_{e^+}|^2 \rho_{el} d^3 r. \tag{2}$$

The basis for employing this technique lies with the fact that the mechanism of Ps atom formation and its subsequent interaction with the medium are highly dependent on the physicochemical properties with locally different electron structure of the environment. Any reorganization in the liquid structure is reflected in abrupt changes in the spectral parameters, e^+/Ps lifetimes and/or intensities as a function of its composition. Reverse micelles have been studied in Sodium AOT–water–isooctane mixtures as a function of AOT concentration, H_2O to AOT mole ratio and temperature using Ps as a probe.[31] The Ps formation probability (the intensity component) has been strongly influenced by micelles formed upon aggregation of nonionic surfactants, Triton-X 100, in aqueous medium. The influence of the electrolyte, nature of the co-surfactant and the solvent on the onset of molecular association and structure of the dispersions containing anionic and cationic surfactants have been extensively studied by Ache *et al.*[32–35] with Ps annihilation and different associative structures existed within the reverse micellar system. Further, important information has been obtained for o-Ps formation probability versus surfactant concentration in the critical micelle concentration range.[36,37]

The interaction of Ps with C_{60} in the solution microenvironment is represented as a donor–acceptor scheme A.

$$2\gamma \xleftarrow{\lambda_p} Ps + C_{60} \underset{k_b}{\overset{k_f}{\leftrightarrow}} [Ps^+ - C_{60}^-] \xrightarrow{\lambda_c} C_{60} + 2\gamma. \tag{A}$$

The [Ps–C_{60}] complex formation results from partial electron transfer from Ps to C_{60}. The presence of a solvent stabilizes the complex to a different degree, depending on the nature of the solvent. k_f and k_b are the forward and backward rate constants, λ_p is the pick-off annihilation rate in pure solvent and λ_c is the annihilation rate from the complex, involving the free, ortho- and para-Ps contributions. The o-Ps contribution, $\lambda_3(1/\tau_3)$ was obtained from the spectral deconvolution of the raw data and was found to vary (Fig. 5) in a concentration range 0.02–2.16 g/dm^3. The high value ($\sim 10^{10}$ M^{-1} s^{-1}) of the calculated overall second-order rate constant (k) suggested that the annihilation occurs from the [Ps–C_{60}] molecular complex and validating the magnitude of λ_3 to be a strong indicative of the solution phase structure of C_{60}. The o-Ps annihilation rate (λ_3) follows a completely different trajectory in the lower concentration range (0.02–0.36 g/dm^3) by going through a minimum (inset of Fig. 5). The critical concentration at the minimum of the curve is obtained as 0.06 g/dm^3. We attribute this critical point to be the onset concentration for

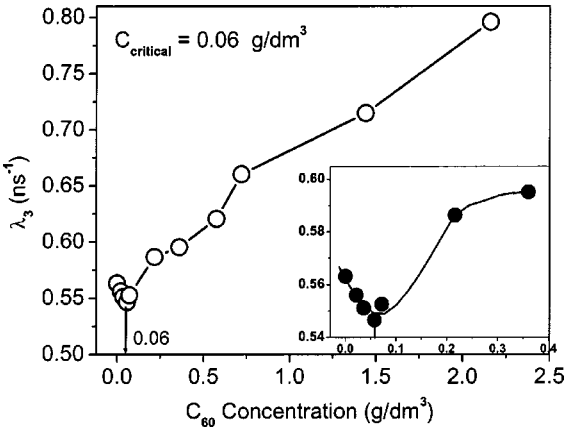

FIG. 5. Variation of the o-Ps annihilation rate (λ_3) with the C_{60} concentration. The critical concentration for C_{60} aggregate formation, indicated by a minimum λ_3 value, is 0.06 g/dm^3. Inset shows an expanded view of the plot near the critical concentration.

stable C_{60} aggregate formation instantaneously upon C_{60} solubilization. At dilute concentrations $<$0.06 g/dm^3, a decreasing trend in the rate/increasing o-Ps lifetime with respect to pure solvent implies a lower magnitude of local electron density around the o-Ps and thus a probable coexistence of C_{60} monomers and pseudo aggregates of much smaller size is inferred, as evident from the TEM experiments. It has been pointed out[2] that at concentrations 3 orders of magnitude lower than the saturation value, clusters practically do not form and isolated fullerene molecules exist in the solution. Beyond $[C]_{critical}$, a sharp enhancement in the rate is representative of the existence of C_{60} clusters in the solution. A close observation of Fig. 5 reveals a slope change between 0.06 and 0.36 g/dm^3 and between 0.36 g/dm^3 and higher concentrations. Beyond 0.36 g/dm^3, because of the increased number density of monomers and the randomly distributed dense C_{60} particles, an increasing electron density annihilates the Ps efficiently, thereby reducing its lifetime. Here, the molecular electrons may screen the e^+e^- Coulomb attraction, resulting in a reduced Ps binding energy, and consequently, a decrease in τ_3 and I_3 at the expense of increasing the free positron intensity (I_2) as was observed in our experiments. Figure 6 shows the o-Ps inten-

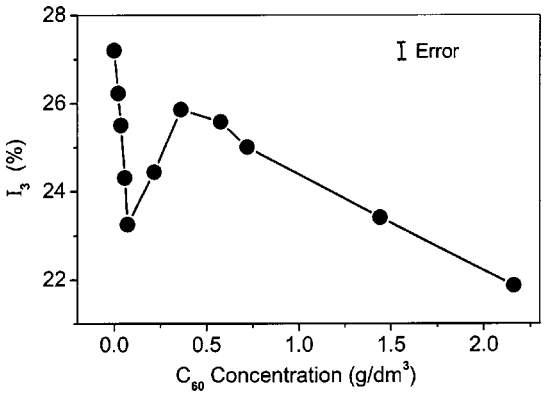

FIG. 6. Variation of the o-Ps intensity (I_3) with concentration of the C_{60} solution.

sity variation over the concentration range studied. The marked lowering in the o-Ps intensity till $[C]_{critical}$ is due to the electron scavenging nature of C_{60} monomer present in this concentration range and has a corresponding match in the annihilation rate profile as shown in Fig. 5.

Although C_{60} is nonionic, the interface between the pseudo-aggregated C_{60} spherical clusters/monomers and the surrounding CS_2 solvent (with finite dipole moment) at concentration <0.06 g/dm^3 can be viewed as a charge-polarized interface. The C_{60} components with a greater polarity act as traps for the quasi-free electrons that form in the positron track and inhibit Ps formation. The possibility of such an interpretation is related to the deeper position of the bottom of the conduction band for quasi-free electrons in the microphase.[38] Further decrease of I_3 at concentrations >0.36 g/dm^3 may be attributed to an enhanced trapping capability arising from the intrinsic polarity of the islands/unevenly distributed aggregates at such concentrations. The latter can create an attractive atmosphere for the charged entity (e^+) moving in a low viscous solvent, leading to its capture and reduction of the Ps yield. Similar o-Ps intensity decrease in Triton–Pentanol aggregates upon water addition was attributed to a transition from swollen micelles to a disclike lamellae structure.[39] Thus, the sharp drops in the o-Ps intensity component at 0.06 and 0.36 g/dm^3 concentrations due to the self-organization in the system imparts a structural rigidity to the solution phase structure of C_{60} and are a sensitive means to determine the onset of aggregation in fullerene systems. Consequently, the annihilation rate λ_3 cannot be the weighted average of the rates of annihilation of thermalized positrons residing in various environments as found in the direct–reverse micellar systems, but will be the annihilation rate from the [Ps–C_{60}] complex. Hence, unlike in micellar systems, our experimental data show as predominant a change in λ_3/τ_3 as that seen in the I_3 values. Association in anionic and cationic dispersion systems have been intensely studied using the ortho-positronium lifetimes and intensities[39–41] and it was reported that the formation of the thermalized Ps atom, i.e., the intensity parameter, is greatly reduced when increasing amount of water becomes solubilized in the reversed micelles formed by sodium bis(2-ethylhexyl) sulfosuccinate in apolar solvents. The application of this technique to potassium oleate–alcohol–oil–water mixture emulsions concluded that a certain water–oil (a long chain aliphatic hydrocarbon, such as hexadecane) ratio is essential for the microemulsion formation. Upon further addition of water, the positron annihilation data sensitively reflected structural rearrangements in these systems, such as the transition from spherical aggregates to disclike lamellae structure. Application of a rigorous diffusion model to a reverse micellar system[42] implied the o-Ps formation to take place in the aqueous part of the micelles, with water aggregates acting as efficient traps.

F. The microscopic diffusion model

In this section, we apply the microscopic diffusion model[42] connecting the o-Ps lifetime in aggregated C_{60} solution with the microscopic parameters of the system such as the C_{60} concentration, the size of the aggregate and its diffusion coefficient, the aggregation number in the cluster, o-Ps formation and its lifetime in the pure solvent and in the C_{60} solutions and its diffusion coefficient. This formulation, which resembles the o-Ps lifetime in porous media[43,44] has been proved successfully with the parameters of sodium dodecyl sulphate (SDS) micellar system and applied to the o-Ps diffusion coefficient determination as a function of temperature in D_2O.[45] The basic features of the model are

(1) Spherical C_{60} aggregates are formed upon diffusion limited cluster aggregation and are in stepwise dynamic equilibrium with the monomer C_{60};
(2) the aggregates are stable during the o-Ps lifetime ($\sim$1 ns);
(3) the C_{60} molecules inside the aggregate are perpendicularly oriented to the aggregate–solvent interface. Thus the average distance between the C_{60} molecules decreases as a result of an increase in the aggregation number. The C_{60} aggregates and o-Ps diffuse in the solvent and the probability of o-Ps getting trapped inside the C_{60} cage at lowest atomic density is $\sim$1;
(4) o-Ps formed in the solvent, may annihilate within the solvent or may reach the aggregate, get trapped and then annihilate;
(5) in the case of o-Ps formation inside the aggregate or its entering the C_{60} aggregate from the solvent, the o-Ps no longer leaves–escapes the aggregation core and its annihilation occurs from the aggregation surrounding.

The fraction of o-Ps formed in the solvent (Q) leads to the fraction formed in the C_{60} aggregate to be 1-Q and the o-Ps annihilates exponentially in the two separate phases. The o-Ps lifetime density function $T_3(t)$ in the aggregated solution is given as

$$T_3(t) = (1-Q)T^c(t) + QT^s(t), \tag{3}$$

where $T^c(t)$ and $T^s(t)$ are the lifetime density functions in the C_{60} cluster aggregate and in the solvent, respectively, with

$$T^c(t) = \lambda_c \exp(-\lambda_c t), \tag{4}$$

where $\lambda_c = 1/\tau_c$. The relative diffusion of o-Ps ($D_{\text{o-Ps}}$) and the aggregate (D_c) takes place pair-wise giving rise to

$$D = D_c + D_{\text{o-Ps}}. \tag{5}$$

Details of the formulation of the model and the solution can be found in Ref. 42. We report here the application of the model with a brief description to the solution of the diffusion problem. The lifetime density function $T_3(t)$ was obtained as

$$T_3(t) = \phi_s(t)\lambda_s \exp(-\lambda_s t) + \phi_c(t)\lambda_c \exp(-\lambda_c t), \tag{6}$$

where $\phi_s(t) = Q\hat{w}_N(t)$ with $\hat{w}_N(t)$ as the probability of finding the o-Ps in the solvent phase. Here ($\hat{}$) implies the configurational average with respect to aggregate coordinates $\vec{r}_1, \vec{r}_2, \ldots, \vec{r}_N$ and

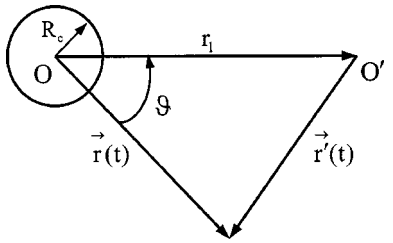

FIG. 7. Boundary conditions for the o-Ps/one aggregate diffusion problem. The origin of the spherical polar coordinate is set to the center of the absorber and the o-Ps atom is assumed to form in O′ at time $t=0$.

$$\theta_c(t)=1-Q\Bigg[\hat{w}_N(t)\exp(-(\lambda_s-\lambda_c)t) + (\lambda_s-\lambda_c)\int_0^t \hat{w}_N(x)\exp(-(\lambda_s-\lambda_c)x)dx\Bigg], \quad (7)$$

where x as a new variable is equal to $\lambda_s(t)$ and N stands for the Nth aggregate.

The mean o-Ps lifetime (τ_p) in the observed C_{60} aggregate solution according to the model is then given by

$$\tau_p=\tau_s'+\tau_c'=\int_0^\infty xT_3(x)dx, \quad (8)$$

where

$$\tau_s'=\int_0^\infty x\phi_s(x)\lambda_s\exp(-\lambda_s x)dx$$

and

$$\tau_c'=\int_0^\infty x\phi_c(x)\lambda_c\exp(-\lambda_c x)dx.$$

For a single aggregate, $N=1$ and in a realistic aggregated solution, $N\gg 1$.

1. o-Ps diffusion in the microscopic environment of a single C_{60} aggregate

In Fig. 7, $\vec{r}(t)$ is the coordinate vector of the center of the aggregate, (R_c) is the aggregate radius and (r_1) is the distance between the center of the cluster and the center of the o-Ps. For a single aggregate, the probability of finding the o-Ps in the solvent at time t for ($r_1>R_c$) is given by

$$w_1(t;r_1,R_c,D)=1-\frac{r_1}{R_c}\mathrm{erfc}\left(\frac{r_1-R_c}{2(Dt)^{1/2}}\right). \quad (9)$$

With the volume element of C_{60} aggregate $<<<$ that of the solvent

$$\tau_p=\tau_s\left[1+\left(\frac{\tau_c}{\tau_s}\right)\rho\exp\left(-\frac{\rho-1}{\Delta^{1/2}}\right)\right], \quad (10)$$

where, $\rho=r_1/R_c$, the dimensionless diffusion coefficient $\Delta=D\tau_s/R_c^2$ and τ_s is the mean o-Ps lifetime in the pure solvent. We have evaluated Eq. (10) and the results are shown in Fig. 8. It is observed that for $\tau_c\geqslant$ or $\leqslant\tau_s$, the mean o-Ps lifetime τ_p observed in presence of a single aggregate is related to that in the solvent τ_s and Δ determines the region around the aggregate where the o-Ps atom must be formed,

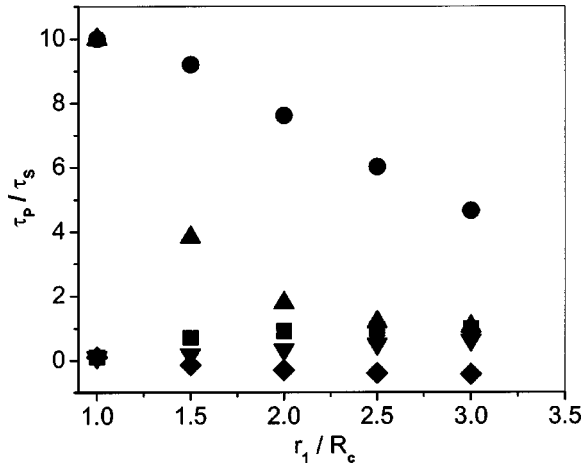

FIG. 8. Effect of the presence of a single C_{60} aggregate on the o-Ps lifetime formed in the solvent at distance r_1 from the aggregate center. τ_p is normalized to τ_s and r_1 to R_c. The Δ value has been varied as 0.1, 1, and 10. ● $\tau_c/\tau_s=10$, $\triangle=1.0$, ▲ $\tau_c/\tau_s=10$, $\triangle=0.1$, ■ $\tau_c/\tau_s=0.1$, $\triangle=0.1$, ▼ $\tau_c/\tau_s=0.1$, $\triangle=1.0$, ◆ $\tau_c/\tau_s=0.1$, $\triangle=10$.

to be able to be absorbed by the aggregate. The size of this region (R_p) is defined as the radius of the sphere where the o-Ps moves in the solvent and is given by $R_p=2(D\tau_s)^{1/2}=2R_c\Delta^{1/2}$, and is calculated to be 13.5 nm in our case. The interaction between the o-Ps and the aggregate occurs with $R_c<r_1<R_c+R_p$. For $r_1>R_p$, no interaction is assumed. τ_s in pure CS_2 was experimentally obtained as 1.775×10^{-9} s. It is difficult to get the exact value of the concentration dependent (D_c) in C_{60} molecular solutions. However, $D=D_c+D_{\text{o-Ps}}$ vide Eq. (5) was used in the above calculation and was estimated to be 2.55×10^{-4} cm^2/s with $D_{\text{o-Ps}}=25.1\times10^{-5}$ cm^2/s from our earlier work[46] and that of the cluster aggregate[47] (D_c) as 2.27×10^{-6} cm^2/s. It has been mentioned that C_{60} cluster formation in solution reduces the diffusion coefficient of an isolated C_{60} molecule (18.5×10^{-5} cm^2/s in CS_2 at 298 K) by 30%. Since the concentration range in which the aggregates are stable is not very large (0.06–0.36 g/dm^3), the D values are almost the same.

2. o-Ps lifetime distribution function in a realistic aggregated C_{60} solution

The boundary conditions for the o-Ps/aggregate diffusion system are depicted in Fig. 9. Here the N-particle function $w_N(t;\vec{r}_1,\ldots,\vec{r}_N)$ is approximated by the product of one-particle functions $w_1(t;\boldsymbol{r}_j)$, $j=1,2,\ldots,N$ and the approximate function depends on the initial aggregate/o-Ps distances $\boldsymbol{r}_j=|\vec{r}_j|$ irrespective of the relative positions of the aggregates. Thus

$$\hat{w}_N(t)=\frac{1}{V^N}\int_V\cdots\int_V w_N(t;r_1,\ldots,r_N)F_N(\vec{r}_1,\ldots,\vec{r}_N) \times d\vec{r}_1,\ldots,d\vec{r}_N. \quad (11)$$

The finite lifetime of o-Ps limits to the volume element V_0 of the volume of the solution in which the o-Ps interacts with the aggregates. Thus, V_0 contains exactly (k) aggregates and its probability $P_k(V_0)$ is given as

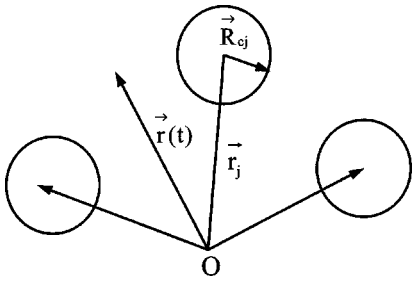

FIG. 9. Boundary conditions for the o-Ps/C_{60} aggregate diffusion problem. The o-Ps is assumed to form at the origin O at $t=0$. The absorber spheres represent the C_{60} aggregates, randomly distributed. $\boldsymbol{r}_j$ is the coordinate vector of the center of the aggregate (j); $R_c=|\boldsymbol{R}_{cj}|$ is the aggregate/cluster radius, $j=1,2,...N$.

$$P_k(V_0)=\frac{(\rho V_0)^k}{k!}\exp(-\rho V_0). \tag{12}$$

The second approximation here is that the aggregate solution is dilute enough such that the aggregates are treated as uncorrelated particles. ρ is the particle density of the aggregates in the solution expressed as $\rho=cN_0/N_{\mathrm{ag}}$ where c is the C_{60} concentration in molarity, N_0 is the Avogadro's number and N_{ag} is the aggregation number. ρV_0 represents the average number of aggregates found in the effective volume V_0, where V_0 is given as $V_0=4\pi/3[(R_c+R_p)^3-R_c^3]$. The configurational average is then given as

$$\hat{w}_N(t)=\exp(-\rho V_0(1-\hat{w}_1(t))). \tag{13}$$

Table II shows these experimental and calculated values. The calculation of the configurational average of w_1 is done by integrating it over the spherical shell drawn around the aggregate with inner and outer radii as R_c and R_c+R_p, respectively, and is given as Eq. (14) below.

$$\hat{w}_1(t)=\hat{w}_1(t;R_c,D)=\frac{3}{(R_c+R_p)^3-R_c^3}\int_{R_c}^{R_c+R_p}x^2 w_1(t;x,R_c,D)dx. \tag{14}$$

In terms of dimensionless variables, $\upsilon=R_p/R_c$, $\varphi=t/\tau_s$ and $\Delta=D\tau_s/R_c^2$

$$w_1(\varphi,\upsilon,\Delta)=1-\frac{3}{(1+\upsilon)^3-1}\left\{[\upsilon(1+\upsilon/2)-\Delta\varphi]\times\mathrm{erfc}\left(\frac{\upsilon}{2(\Delta\varphi)^{1/2}}\right)-2\left(\frac{\Delta\varphi}{\pi}\right)^{1/2}\right\}\times\left[\left(1+\frac{\upsilon}{2}\right)\exp\left(-\frac{\upsilon^2}{4\Delta\varphi}\right)-1\right]+\Delta\varphi. \tag{15}$$

In this calculation, we have taken $t=10^{-6}$ s, corresponding to the time of attachment of 2 C_{60} clusters of comparable size under a diffusion limited aggregation approach[45] as discussed in the TEM section. Further, since the diffusion model is based on the assumption that the o-Ps atoms formed in the solvent are found there at time $t=0$, an interaction between o-Ps and the C_{60} aggregate is justified. With $t=10^{-6}$ s, it follows that $0<\hat{w}_1(t;R_c,D)<1$ for the stable concentration range 0.06–0.36 g/dm^3. The $\hat{w}_N(t;R_c,D)$ values for these concentrations are listed in Table II. Using these, we calculated the mean o-Ps lifetime[42] in the C_{60} aggregate solution as

$$\frac{\tau_p}{\tau_s}=\frac{\tau_c}{\tau_s}[1-Q\mu_0(1-\tau_s/\tau_c)], \tag{16}$$

where

$$\mu_0=\int_0^\infty \hat{w}_N(x,\upsilon,\Delta)\exp(-x)dx, \tag{17}$$

and Q is the volume fraction of the solvent, expressed by the partial molar volume ν_m of C_{60} as $Q=1-\nu_m$. With the reported ν_m of C_{60} in CS_2 solution[48] to be 350.6 cm^3/mol (did not vary substantially with concentration, for solvents toluene, o-xylene, etc.), the calculated τ_p/τ_s values, according to Eqs. (16) and (17), in the desired concentration range are listed in Table II, consequent to the evaluation of $\hat{w}_N$, vide Eqs. (13) and (15). Figure 10 depicts the experimental and calculated o-Ps lifetimes, τ_p/τ_s (normalized to that of pure solvent) versus the C_{60} concentration with $\tau_c/\tau_s=0.5$ and 2.0 for the dimensionless diffusion coefficient $D\tau_s/R_c^2=10^{-2}$, the latter complying with the experimental values of D, τ_s, and R_c.

An excellent agreement between the experimental and the calculated o-Ps lifetimes implies the validity of the diffusion model to the stable cluster aggregates in CS_2 medium with the following important conclusions:

TABLE II. Experimental and calculated values of the C_{60} aggregation parameters in CS_2 solutions as a function of concentration.

$[C_{60}]$ (g/dm^3)	τ_p/τ_s (Expt.)	n	R_c (nm)	$\hat{w}_N(t)$	$\frac{D\tau_s}{R_c^2}$	$\tau_p(\mathrm{cald})/\tau_s$ ($\tau_c/\tau_s=0.5$)	$\tau_p(\mathrm{cald})/\tau_s$ ($\tau_c/\tau_s=2$)
0.06	1.03	3.2×10^4	125	0.999	0.012	1.0	1.01
0.14	0.96	2.5×10^4	110	0.997	0.015	0.96	1.08
0.36	0.94	1.7×10^4	90	0.992	0.022	0.93	1.15

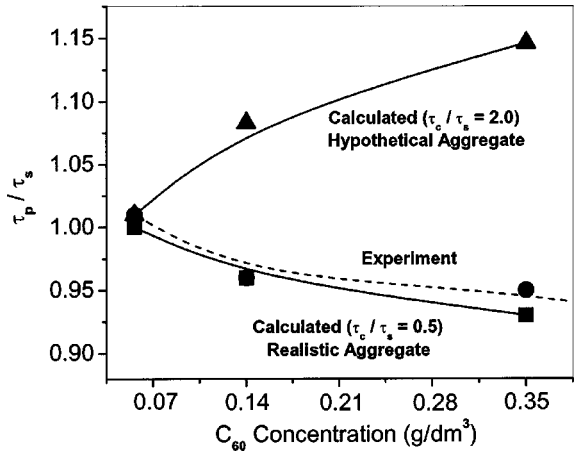

FIG. 10. The experimental and calculated o-Ps lifetimes (normalized to that in the solvent) vs concentration of C_{60} in the aggregate solutions. The dimensionless diffusion coefficient $D\tau_s/R_c^2 = 10^{-2}$.

(1) The diffusion coefficients of o-Ps and the C_{60} aggregate as 25.1×10^{-5} cm^2/s and 2.27×10^{-6} cm^2/s, respectively, are validated.
(2) The model calculation of o-Ps lifetimes fit with the experimental data for C_{60} aggregates in CS_2 solution for $\tau_c/\tau_s = 0.5$ [Fig. 10, realistic aggregate with $\tau_c/\tau_s = 0.5$], implying the o-Ps lifetime in the C_{60} aggregate phase to be half as that of the pure solvent CS_2, if the o-Ps were to annihilate in individual phases. This indicates a higher electron density around the C_{60} aggregate than the CS_2 solvent, which is expected and adds to further confirmation of a successful application of the model. This is in contrast to the micellar environments where realistic aggregates were obtained[42] with $\tau_m/\tau_s = 2.0$ with the low atomic/electron density region of the micellar boundary serving as an effective o-Ps trap. This work thus provides ample scope for a new aggregated system and to focus on the solution phase structure of the C_{60}.

IV. CONCLUSION

A microscopic diffusion model, calculating the o-Ps lifetimes in C_{60} aggregated solutions in CS_2 solvent was adopted. An excellent agreement between the calculated and experimental o-Ps lifetimes in the aggregated solutions reflected on important quantitative parameters of the system. These findings followed the concentration dependent structure attribution to the C_{60} aggregates obtained from a microscopic picture of the Ps surroundings in the C_{60} solution and from TEM. Existence of several competing mechanisms during solubilization were observed and an increasing interaction between the C_{60} molecules resulted in a displacement of equilibrium towards the solid state. At dilute concentrations, before the critical point, the system remained as an isotropic liquid with C_{60} monomers, along with monomers tending to aggregate but failing to achieve stability or attainment of an equilibrium state owing to low concentration, accompanied by large solute–solvent interactions. At intermediate concentrations, just at or after the onset of aggregation, the clusters seemed highly immobilized owing to strong intermolecular interactions. On attaining the full cluster growth and at a higher concentration, the rigidity of the cluster core was greatly reduced and the properties of the cluster approached that of the bulk, accompanied by a phase separation.

ACKNOWLEDGMENTS

This work has been supported by the Department of Science and Technology (DST), Government of India, Grant No. SP/S1/H-33/95. A.D.B. thanks the DST, Govt. of India for a Research Fellowship.

[1] Q. Ying, J. Marecek, and B. Chu, J. Chem. Phys. **101**, 2665 (1994).
[2] V. N. Bezmel'nitsyn, A. V. Eletskii, and E. V. J. Stepanov, J. Phys. Chem. **98**, 6665 (1994).
[3] Q. Ying, J. Marecek, and B. Chu, Chem. Phys. Lett. **219**, 214 (1994).
[4] R. G. Alargova, S. Deluchi, and K. Tsujii, J. Am. Chem. Soc. **123**, 10460 (2001).
[5] S. Nath, H. Pal, D. K. Palit, A. V. Sapre, and J. P. Mittal, J. Phys. Chem. B **102**, 10158 (1998).
[6] L. A. Bulavin, I. I. Adamenko, V. M. Yashchuk, T. Ogul'chansky, Y. I. Prylutskyy, S. S. Durov, and P. Scarff, J. Mol. Liq. **93**, 187 (2001).
[7] S. Nath, H. Pal, and A. V. Sapre, Chem. Phys. Lett. **327**, 143 (2000).
[8] N. P. Yevlampieva, Y. F. Birulin, E. V. Melenevskaja, V. N. Zgonnik, and E. I. Rjumtsev, Colloids Surf., A **209**, 167 (2002).
[9] R. S. Ruoff, R. Malhotra, and D. L. Huestis, Nature (London) **361**, 140 (1993).
[10] Y-P. Sun and C. E. Bunker, Nature (London) **365**, 398 (1993).
[11] H. N. Ghosh, A. V. Sapre, and J. P. Mittal, J. Phys. Chem. **100**, 9439 (1996).
[12] V. N. Bezmel'nitsyn, A. V. Eletskii, and E. V. J. Stepanov, in *Progress in Fullerene Research*, edited by H. Kuzmany (World Scientific, Singapore, 1994), p. 45.
[13] J. S. Ahn, K. Suzuki, Y. Iwasa, N. Otsuka, and T. Mitani, J. Lumin. **76/77**, 201 (1998).
[14] A. D. Bokare and A. Patnaik, J. Phys. Chem. B **107**, 6079 (2003).
[15] P. Kirkegaard, M. Eldrup, E. Mogensen, and N. Y. Pedersen, Comput. Phys. Commun. **23**, 307 (1989).
[16] J. Forsman, J. P. Harrison, and A. Rutenberg, Can. J. Chem. **65**, 767 (1987).
[17] J. H. Lee, G. Beaucage, S. E. Pratsinis, and S. Vemury, Langmuir **14**, 5751 (1998).
[18] C. M. Sorensen, Aerosol Sci. Technol. **35**, 648 (2001).
[19] P. Mukherjee, J. Phys. Chem. **76**, 565 (1972).
[20] C. Cametti, P. Codastefano, and P. Tartaglia, Phys. Rev. A **36**, 4916 (1987).
[21] Z. Zhou and B. Chu, J. Colloid Interface Sci. **143**, 356 (1991).
[22] J. E. Martin, Phys. Rev. **36**, 3415 (1987).
[23] P. Meakin, Phys. Rev. A **27**, 2616 (1983).
[24] M. Lattuada, H. Wu, and M. Morbidelli, Phys. Rev. E **64**, 061404 (2001).
[25] R. D. Mountain and G. W. Mulholland, Langmuir **4**, 1321 (1988).
[26] A. Das, S. Dhara, and A. Patnaik, Phys. Rev. B **59**, 11069 (1999).
[27] N. Asherie, A. Lomakin, and G. B. Benedek, Phys. Rev. Lett. **77**, 4832 (1996).
[28] M. Takata, Y. Kubota, M. Sakata, J. Harada, H. Saito, H. Shinohara, H. Nagashima, and Y. Ando, *Presented at Physical Society of Japan*, 1991 (unpublished).
[29] P. A. Forsyth, S. Marcedja, D. J. Mitchell, and B. W. Ninham, Adv. Colloid Interface Sci. **9**, 37 (1978).
[30] M. Adams, Z. Dogic, S. L. Keller, and S. Fraden, Nature (London) **393**, 349 (1998).
[31] M. F. F. Marques, H. D. Burrows, M. D. Miguel, A. P. Lima, C. L. Gil, and G. Duplatre, J. Phys. Chem. **100**, 7595 (1996).
[32] A. Boussaha, B. Djermouni, L. A. Fucugauchi, and H. J. Ache, J. Am. Chem. Soc. **102**, 4654 (1980).
[33] A. Boussaha and H. J. Ache, J. Phys. Chem. **85**, 1683 (1981).
[34] Y. C. Jean and H. J. Ache, J. Am. Chem. Soc. **99**, 7504 (1977).
[35] Y. C. Jean and H. J. Ache, J. Phys. Chem. **82**, 811 (1978).
[36] H. J. Ache, in *Positron Annihilation*, edited by P. G. Coleman, S. C. Sharma, L. Diana (North-Holland, Amsterdam, 1982), p. 773.

[37] Y. C. Jean and H. J. Ache, J. Am. Chem. Soc. **100**, 984 (1979).
[38] V. I. Grafutin and E. P. Prokopev, Phys. Usp. **45**, 59 (2002).
[39] A. Boussaha, B. Djermouni, L. A. Fucugauchi, and H. J. Ache, J. Am. Chem. Soc. **102**, 4654 (1980).
[40] A. Boussaha and H. J. Ache, J. Phys. Chem. **85**, 1683 (1981).
[41] S. K. Das and B. N. Ganguly, J. Radioanal. Nucl. Chem. **230**, 17 (1998).
[42] S. Vass, J. Phys. Chem. **90**, 1099 (1986).
[43] W. Brandt and R. Paulin, Phys. Rev. Lett. **21**, 193 (1968).
[44] W. Brandt and R. Paulin, Phys. Rev. B **5**, 2430 (1972).
[45] S. Vass, Z. Kajcsos, and B. Molnar, Chem. Phys. Lett. **118**, 105 (1985).
[46] A. D. Bokare and A. Patnaik (unpublished).
[47] V. N. Bezmel'nitsyn, Phys. Usp. **41**, 1091 (1998).
[48] P. Ruelle, A. Farina-Cuendet, and U. W. Kesselring, J. Am. Chem. Soc. **118**, 1777 (1999).